

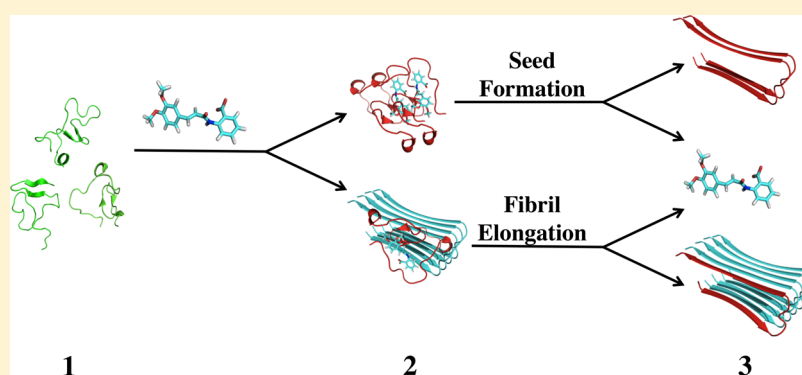
Tranilast Binds to $A\beta$ Monomers and Promotes $A\beta$ Fibrillation

Christopher R. Connors,^{†,‡} David J. Rosenman,^{†,⊥} Dahabada H. J. Lopes,[∇] Shivina Mittal,[∇] Gal Bitan,^{∇,§,‡} Mirco Sorci,^{†,||} Georges Belfort,^{†,||} Angel Garcia,^{†,○} and Chunyu Wang^{*,†,‡,⊥}

[†]Center for Biotechnology and Interdisciplinary Studies, [‡]Graduate Program in Biochemistry and Biophysics, [⊥]Department of Biology, ^{||}Department of Chemical and Biological Engineering, and [○]Department of Physics, Rensselaer Polytechnic Institute (RPI), Troy, New York 12180, United States

[∇]Department of Neurology, David Geffen School of Medicine, [§]Brain Research Institute, and [‡]Molecular Biology Institute, University of California at Los Angeles, Los Angeles, California 90095, United States

S Supporting Information



ABSTRACT: The antiallergy and potential anticancer drug tranilast has been patented for treating Alzheimer's disease (AD), in which amyloid β -protein ($A\beta$) plays a key pathogenic role. We used solution NMR to determine that tranilast binds to $A\beta$ 40 monomers with $\sim 300 \mu\text{M}$ affinity. Remarkably, tranilast increases $A\beta$ 40 fibrillation more than 20-fold in the thioflavin T assay at a 1:1 molar ratio, as well as significantly reducing the lag time. Tranilast likely promotes fibrillation by shifting $A\beta$ monomer conformations to those capable of seed formation and fibril elongation. Molecular docking results qualitatively agree with NMR chemical shift perturbation, which together indicate that hydrophobic interactions are the major driving force of the $A\beta$ –tranilast interaction. These data suggest that AD may be a potential complication for tranilast usage in elderly patients.

Alzheimer's disease (AD) accounts for 60–80% of all dementia cases, affecting ~ 5.3 million people in the United States alone.¹ AD is pathologically characterized by neurofibrillary tangles and senile plaques. The major component of senile plaques is aggregated, fibrillar, insoluble $A\beta$. $A\beta$ is a cleavage product of the amyloid precursor protein (APP). First, β -secretase cleaves APP at what will be the N-terminus of $A\beta$, followed by γ -secretase cleavage to generate the C-terminus of $A\beta$. The most common forms of $A\beta$ are 40 and 42 amino acid residues in length and are called $A\beta$ 40 and $A\beta$ 42, respectively. $A\beta$ 42 aggregates much faster than $A\beta$ 40 and is more toxic. Though $A\beta$ is considered benign in its monomeric form,^{2–4} $A\beta$ fibrils,^{5–7} protofibrils,⁸ and various oligomers including dimers,⁹ trimers,¹⁰ and 12-mers^{11,12} are toxic, and their presence in the AD brain correlates with the clinical manifestation of dementia.^{13–15}

Tranilast is a small molecule currently marketed in Korea and Japan as an antiallergy drug. It is being investigated for a wide variety of other uses,¹⁶ from reducing the pathological fibrosis associated with myocardial infarctions,¹⁷ to reducing human breast cancer cell migration and colony formation.¹⁸ The drug is particularly promising as a potential anticancer agent¹⁹ due to its antiproliferative effects in prostate,²⁰ breast,²¹ and pancreatic

cancers.²² Usage of tranilast and its derivatives in the treatment of neurodegenerative conditions, including AD, has been patented.²³ Oral administration of tranilast inhibited the growth of rat gliomas *in vivo*, suggesting tranilast can cross the blood–brain barrier.²⁴ Tranilast also had an antiapoptotic effect on neurons and increased neurogenesis, both in a dose-dependent manner.²³ Given tranilast's potential use in the treatment for AD, we decided to explore its possible interaction with $A\beta$.

We combined NMR, aggregation assays, and docking simulations to study the tranilast– $A\beta$ interaction in a multidisciplinary approach. First, NMR spectroscopy was used to study tranilast's interaction with monomeric $A\beta$ and to map tranilast's binding site on the $A\beta$ monomer with residue-specific resolution. Second, ThT fluorescence and dot blots with the antioligomer antibody A11 determined tranilast's effect on $A\beta$ self-assembly. Fibril morphology was confirmed using atomic force microscopy (AFM). Finally, molecular docking of tranilast to REMD-simulated structures of

Received: April 5, 2013

Revised: May 16, 2013

Published: May 16, 2013

$A\beta$ was applied to gain further insight into the interaction between tranilast and $A\beta$.

MATERIALS AND METHODS

NMR Experiments. NMR samples were made from ^{15}N -labeled, HFIP-treated $A\beta_{40}$ or $A\beta_{42}$ (rPeptide, Bogart, GA, USA). Peptide films were resuspended in 1 mL of 10 mM NaOH. Aliquots of 125 μL were then added to 20 mM potassium phosphate, pH 7.3, and 10% D_2O to prepare initial NMR samples for titration. Tranilast was purchased from Cayman Chemical and solubilized in either DMSO or $\text{DMSO-}d_6$ to create a stock solution of 20 mg/mL. Chemical shift perturbation (CSP) was monitored using ^{15}N - ^1H -HSQC spectra at increasing molar ratios of tranilast to $A\beta$. A control sample of DMSO without tranilast was also titrated into $A\beta$ samples and CSP due to the addition of DMSO was subtracted from CSP observed during tranilast titrations. CSP was calculated as $\Delta\delta = ((10\Delta\delta_{\text{H}})^2 + (\Delta\delta_{\text{N}})^2)^{1/2}$. All NMR experiments were performed on an 800 or 600 MHz spectrometer equipped with a cryogenic probe at 277 K, to minimize the aggregation of $A\beta$. This protocol of $A\beta$ sample preparation and NMR setup ensures that NMR signals are from $A\beta$ monomers.^{25,26} CSP values were fitted to the following equation to determine K_{d} for the $A\beta$ /tranilast interaction:

$$\Delta\delta_{\text{obs}} = \Delta\delta_{\text{max}} \left\{ \frac{([P]_{\text{t}} + [L]_{\text{t}} + K_{\text{d}}) - \sqrt{([P]_{\text{t}} + [L]_{\text{t}} + K_{\text{d}})^2 - 4[P]_{\text{t}}[L]_{\text{t}}}}{2[P]_{\text{t}}} \right\}$$

where $\Delta\delta_{\text{obs}}$ is observed CSP of $A\beta$, $\Delta\delta_{\text{max}}$ is the CSP of $A\beta$ in the bound state, $[P]_{\text{t}}$ is total $A\beta$ peptide concentration, $[L]_{\text{t}}$ is total ligand concentration, and K_{d} is the dissociation constant.

Thioflavin T (ThT) Assay and Dot Blot. For aggregation experiments, samples of HFIP-treated $A\beta_{40}$ or $A\beta_{42}$ first were resuspended to 1 mg/mL in DMSO, then diluted in PBS to a final concentration of 20 μM and incubated at 37 $^{\circ}\text{C}$. ThT assays were performed in triplicate to measure fibril formation using 50 μL of incubated sample and 350 μL of 10 μM ThT in 50 mM glycine, pH 8.0. Samples were excited at 440 nm and emission at 485 nm was measured using a Hitachi F-4500 fluorescence spectrophotometer (Hitachi High-Technologies Co, Tokyo, Japan). Dot blots were performed using the oligomer-specific antibody A11 (Invitrogen, Carlsbad, CA, USA) and the WesternBreeze Chemiluminescent kit (Invitrogen, Carlsbad, CA, USA). Blots were visualized on a ChemiDoc MP system (Bio-Rad, Hercules, CA, USA).

Atomic Force Microscopy (AFM). Aggregated samples of $A\beta$ were prepared in the same manner as for the ThT assay. For each sample, 20 μL was placed on a mica surface for adsorption for 5 min. Nonadsorbed protein was washed away with abundant water. Three-dimensional measurements at the nanometer scale were collected in air using the tapping mode technique with an MFP-3D atomic force microscope (Asylum Research, Santa Barbara, CA, USA) and standard Si cantilevers (AC240TS, Olympus America Inc., Center Valley, PA, USA). Images were then analyzed with Igor Pro 6 (WaveMetrics, Inc., Lake Oswego, OR, USA).

Molecular Docking. Tranilast was docked onto previously published centroid structures from all-atom REMD simulations of $A\beta_{40}$.²⁷ The structure of tranilast was obtained from the PubChem database (CID: 5282230)²⁸ and subsequently minimized in vacuo with MOE²⁹ by using the MMFF94x force field (a modified version of MMFF94s³⁰), stopping at a gradient of 10^{-3} . This ligand structure was blindly docked onto each $A\beta$ centroid MOE's docking feature²⁹ with the entire centroid as the receptor structure. Placement was done using the triangle matcher algorithm.

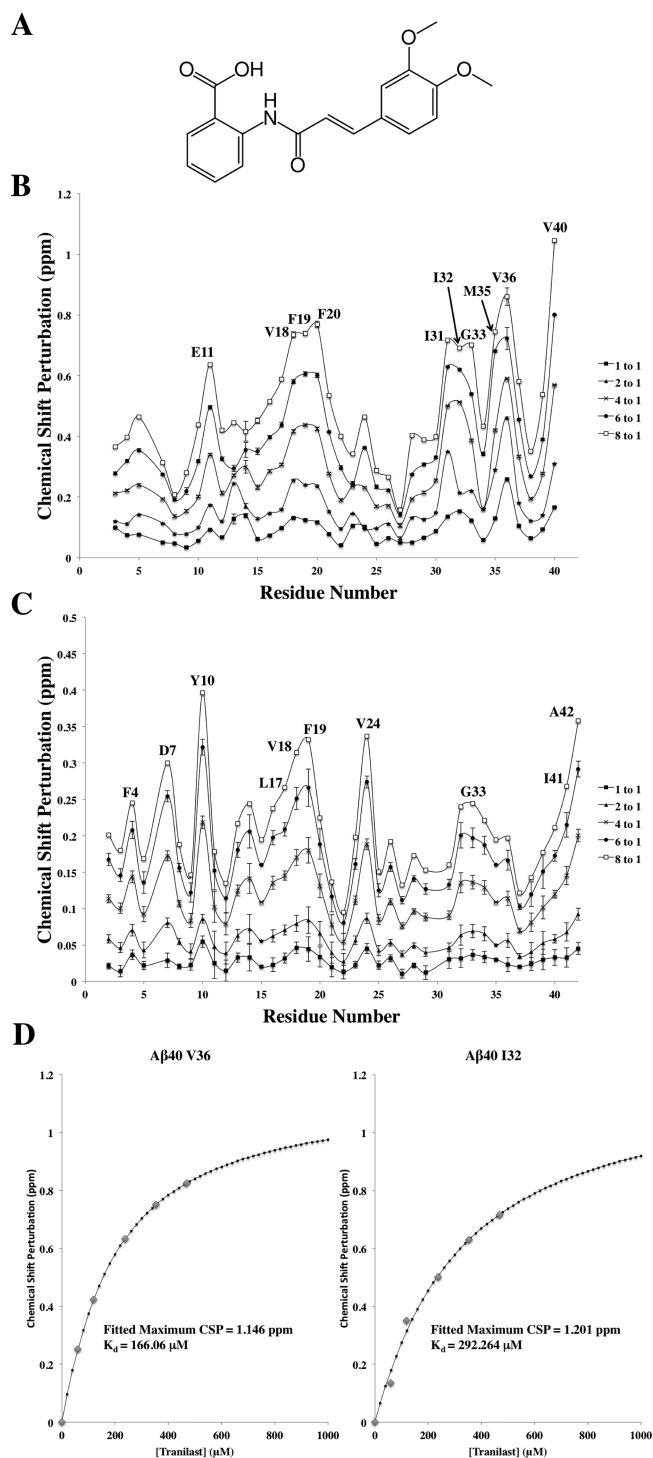


Figure 1. NMR chemical shift perturbations due to tranilast binding to $A\beta_{40}$ or $A\beta_{42}$. (A) A 2D representation of tranilast, which was titrated from 1 to 8 mol equiv of (B) $A\beta_{40}$ and (C) $A\beta_{42}$. CSP was calculated as $\Delta\delta = ((10\Delta\delta_{\text{H}})^2 + (\Delta\delta_{\text{N}})^2)^{1/2}$, where $\Delta\delta_{\text{H}}$ and $\Delta\delta_{\text{N}}$ are CSPs of amide proton and nitrogen, respectively. The 10 residues with the largest CSP in each peptide are labeled. $A\beta_{40}$ CSP due to tranilast was much greater than that of $A\beta_{42}$, suggesting greater affinity for $A\beta_{40}$. (D) Examples of fitted K_{d} curves calculated using CSP. Samples of $A\beta$ monomer were prepared at 60 μM in 20 mM potassium phosphate (pH 7.3) and 10% D_2O . All NMR experiments were carried out at a temperature of 277 K.

The top 30 best placements (according to London dG scores) were refined with minimization (stopping at a gradient 10^{-3}) using the OPLS-AA force field with Born solvation. The top scoring pose

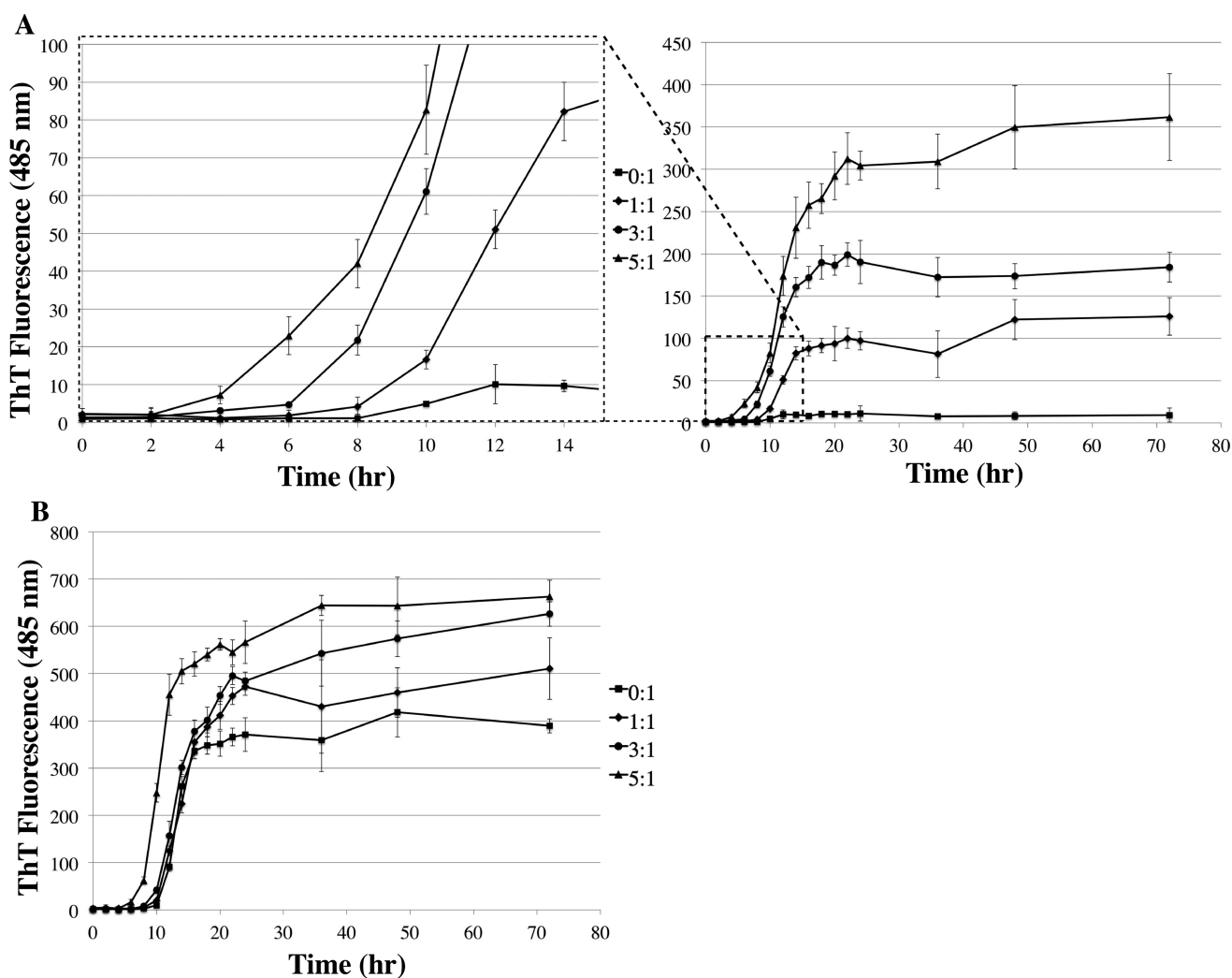


Figure 2. Tranilast promotes A β fibrillation. ThT assay measuring the effect of varying molar ratios (0:1, 1:1, 3:1, 5:1) of tranilast to A β on fibril formation. (A) Tranilast significantly increased A β 40 maximum fibrillation in a dose-dependent manner. There was also a significant decrease in the lag phase between 1:1 and 3:1, and 3:1 and 5:1 molar ratios of tranilast to A β 40. (B) Tranilast significantly increased A β 42 fibrillation, though the effect was less pronounced. The assay was carried out in triplicate with 20 μ M A β in PBS + 5% DMSO, incubated at 37 $^{\circ}$ C without agitation. Error bars represent ± 1 standard deviation.

(after rescoring with the London dG algorithm) was then retained. Residue-indexed surface area of contact between A β and tranilast for each of the MOE docks were calculated using LPC software.³¹

RESULTS

Chemical Shift Perturbation. NMR titrations of tranilast into ¹⁵N-labeled A β 40 or A β 42 yielded residue-specific chemical shift perturbation (CSP) (Figure 1). The greatest CSP was observed at the C-terminus of both A β 40 and A β 42. Relatively large CSP was also observed in regions comprising residues 11–21 and 30–37 in A β 40, and to a lesser extent, in similar regions of A β 42. Largest CSP are observed for residues E11, V18, F19, F20, I31, I32, G33, M35, V36, and V40. These residues are largely nonpolar, indicating that hydrophobic interaction may play a key role in tranilast binding to A β . CSP in A β 40 was found to be substantially greater than in A β 42. ¹H and ¹⁵N perturbations for tranilast at 0–8 molar ratio equivalents were then fit to determine the K_d values for the tranilast–A β interaction. Because of the low affinity of binding between A β and tranilast and limitation of tranilast solubility in aqueous solution, titrating A β to near complete saturation was not possible.

For the A β 40–tranilast interaction, CSP fittings for residues I31, I32, and V36, where the titration is closer to saturation and there was apparent curvature in the fitted titration curve, were used to calculate an average K_d 0.31 ± 0.13 mM. For A β 42–tranilast interaction, due to the lower affinity, none of the residues were titrated close to saturation. But for a comparison with A β 40, the average K_d of the three residues in A β 42 with lowest apparent K_d (F4, Y10, and G33) was 2.4 ± 0.2 mM, still significantly higher than the measured K_d for A β 40.

Aggregation Assays and AFM. To further confirm the A β –tranilast interaction and to probe how tranilast affects A β self-assembly, we carried out ThT assays to study A β β -sheet formation, and dot blots with antibody A11 to study A β oligomer formation. AFM was used to confirm aggregate morphology.

Despite the measured millimolar affinity of tranilast to A β 40 and A β 42, there was a significant effect of tranilast binding on A β fibrillation. ThT assays of A β 40 and A β 42 both showed significant increases in fibril formation with the addition of tranilast (Figure 2). There was nearly no increase in ThT fluorescence for A β 40 in the absence of tranilast, whereas the addition of 1 equiv of tranilast caused more than a 20-fold increase

in maximum ThT signal (Figure 2A). This increase was dose-dependent up to a 5:1 molar ratio, the highest ratio tested. There was also a significant decrease in the lag phase of fibril formation between 1:1 and 3:1, as well as between 3:1 and 5:1 molar ratios of tranilast to $A\beta$ 40 (Figure 2A). This decrease in the lag phase suggests tranilast not only increased the overall amount of fibrils formed but also promoted formation of fibril seeds. The effect on $A\beta$ 42 fibril formation was less pronounced (Figure 2B), with only a \sim 1.7-fold increase in maximum ThT signal at a molar ratio of 5:1, possibly due to the greater affinity of tranilast for $A\beta$ 40 and the faster aggregation propensity of $A\beta$ 42 on its own.

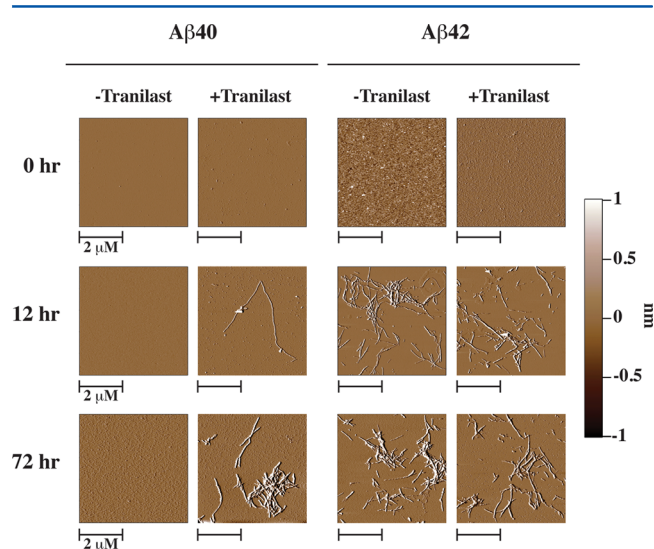


Figure 3. AFM images of $A\beta$ 40 and 42 samples incubated with either 0:1 (–Tranilast) or 5:1 (+Tranilast) molar ratios of tranilast to $A\beta$. No fibrils were observed at 0 h for any sample. After 12 h, fibrils were observed in both $A\beta$ 42 samples, and only a sparse amount of fibrils were observed in the $A\beta$ 40 sample with tranilast. After 72 h of incubation at 37 °C, more fibrils were observed in the $A\beta$ 40 sample containing tranilast and in both $A\beta$ 42 samples. No fibrils were observed in the $A\beta$ 40 without tranilast at any point. AFM samples were prepared from 20 μ M $A\beta$ in PBS + 5% DMSO, incubated at 310 K without agitation, in either the presence or absence of 100 μ M tranilast.

To confirm that the increase in ThT signal was due to increased fibril formation, we observed $A\beta$ samples with AFM. These samples were prepared under the same conditions as the samples for the ThT assay. No fibrillar aggregates were observed in the initial $A\beta$ samples, both with and without 100 μ M tranilast. Additionally, fibrils were not observed in the $A\beta$ 40 without tranilast at any time point, consistent with the very small change in ThT signal. After incubation at 37 °C for 12 h, fibrils formed in both $A\beta$ 42 samples. To a lesser extent, fibrils formed in the $A\beta$ 40 sample with tranilast. After 72 h, the time where ThT signal plateaued fibrils were seen to form in both $A\beta$ 42 samples and $A\beta$ 40 with tranilast, a result consistent with the significant increases in ThT signal observed for these samples.

To determine if tranilast was incorporated into the $A\beta$ fibrils, we used 1 H NMR on disaggregated fibril samples formed in the presence of tranilast. Fibril samples were first centrifuged. The supernatant was then decanted, leaving only precipitated fibrils, which were washed with PBS two times and then resuspended in disaggregation buffer (8 M urea, 20 mM potassium phosphate, pH 7.3). 1 H NMR spectra were then recorded of the

disaggregated samples to determine the presence of tranilast signal. 1 H NMR showed no tranilast signal in the disaggregated fibril samples, while there was clear signal for disaggregated $A\beta$ monomers (data not shown). Therefore, tranilast was not incorporated into $A\beta$ fibrils formed in its presence.

All dot blots were used to study $A\beta$ oligomer formation in the absence or presence of tranilast (Figure 4). There was no

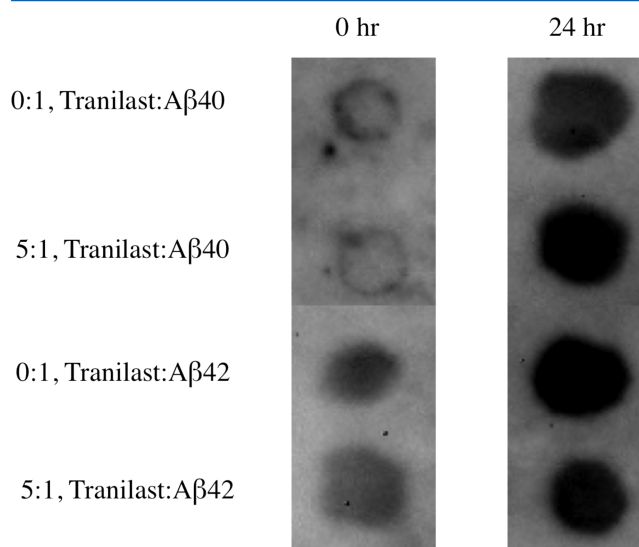


Figure 4. $A\beta$ dot blots with oligomer-specific antibody A11 in the absence or presence of tranilast. At a 5:1 molar ratio of tranilast to $A\beta$, after 24 h of incubation at room temperature without agitation, there is no significant difference in oligomer formation between samples containing tranilast and control samples. Samples consisted of 20 μ M $A\beta$ in PBS + 5% DMSO.

noticeable difference in oligomer formation between the samples containing tranilast and control samples, suggesting that tranilast binding did not affect $A\beta$ 40 or $A\beta$ 42 A11-active oligomerization.

Molecular Docking Studies. To further probe the binding modes of tranilast's interaction with $A\beta$, we employed molecular docking with centroid structures of $A\beta$ 40 derived from replica exchange molecular dynamics (REMD) in explicit water that have been validated by NMR-observed constraints.²⁷ The many structures from these simulations were grouped into clusters comprising structures within a 3 Å RMSD cutoff for $A\beta$ 40.²⁷ These clusters were then represented by a centroid structure, which had the lowest RMSD to all members within the cluster. Using MOE, we docked tranilast to two centroid structures representing \sim 30% of all simulated $A\beta$ 40 structures (Figure 5).

We found qualitative agreement between the binding sites determined by NMR and *in silico* docking. Residues Y10, E11, L17, V18, F19, G29, A30, I31, I32, G33, L34, M35, V36, and G37 are in direct contact with tranilast, with atoms within 5 Å of tranilast (Figure 5), as calculated by LPC software.³¹ These residues all exhibited amide CSP greater than 0.3 ppm in the presence of 6 mol equiv of tranilast (Figure 1). Among the 12 residues with largest CSP, indicated in Figure 1B, 10 could be explained by their proximity to tranilast in Figure 5. Significant CSP of other two residues, F20 and V40, could not be explained by docking results.

Docking revealed key interactions that drive $A\beta$ –tranilast binding (Figure 5). The side chain of I32 interacted with the benzoic acid ring of tranilast, while the side chain of I31 showed a similar interaction with the other aromatic ring of tranilast.

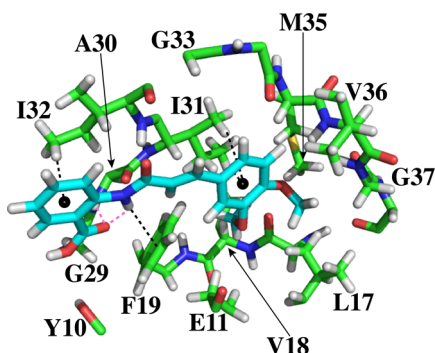


Figure 5. Binding pocket from the top scoring docking simulation produced by MOE between tranilast and the two most representative centroids of $A\beta_{40}$. Only $A\beta$ atoms (carbon in green, oxygen in red, nitrogen in blue, and hydrogen in white) within 5 Å of tranilast (carbon in cyan, oxygen in red, nitrogen in blue, and hydrogen in white) are depicted. Black dashed lines indicate π -H interactions. Magenta dashed lines indicate hydrogen bonds. This docking pose was the highest scoring dock to tranilast among all of the docks determined for both of the $A\beta$ centroids used.

There was a π -H interaction between the aromatic ring of F19 and the amide group of tranilast. In addition, there was bifurcated hydrogen bonding between the carboxylic acid group of tranilast to its own amide group and to the amide of A30.

DISCUSSION

Implication for Clinical Use of Tranilast in Patients at Risk for AD. The patent for tranilast’s use in neurodegenerative diseases is based on its antiapoptotic and pro-neurogenesis effects regardless of the presence of $A\beta$.²³ Given its potential use in the treatment of neurodegenerative diseases and in other diseases commonly affecting elderly patients (e.g., cancer^{18–21,32–44}), the characterization of tranilast’s interaction with $A\beta$ is important. The toxic effect of $A\beta$ fibrils in AD patients is well documented.⁴⁵ An increase in fibrilization of $A\beta_{40}$ in particular due to tranilast could lead to elevated cerebral amyloid

angiopathy and become a devastating side-effect. We showed that there is a ~ 20 -fold increase in $A\beta$ fibril formation in the presence of an equimolar amount of tranilast, as well as a significant increase in fibril seeding. Thus, in treating elderly patients with tranilast, new signs or the aggravation of dementia need to be carefully monitored. Ideally, a statistical analysis in elderly patient population should be carried out to ascertain whether tranilast indeed affects the onset and progression of AD.

Mechanism of Tranilast Promotion of $A\beta$ Fibrillation. Although tranilast binds $A\beta$ monomers with low affinity, it significantly increases $A\beta_{40}$ fibrillation. These \sim millimolar binding affinities of tranilast to both $A\beta_{40}$ and 42 monomers are in a range that is traditionally considered too weak for effective drug interaction. However, taking into account that IDPs, such as $A\beta$, sample a large number of conformations, drugs like tranilast may only bind certain populations of conformations with relatively high affinity. The observed binding affinities reflect binding to all monomer conformations, including those that do not bind, and thus may be deceptively low. These observed low binding affinities also do not necessarily correlate with the extent of the effect of binding on aggregation, as is the case with tranilast and $A\beta_{40}$. Alternatively, tranilast may bind to most $A\beta$ monomer conformations with low affinity, although this is unlikely given its significant effects on fibrillation. Because tranilast is not present in the fibrils and does not affect A11-reactive oligomer formation, the effect on fibrillation likely stems from binding of tranilast to $A\beta$ monomer conformations that favor fibril formation, shifting the thermodynamic equilibrium of sampled conformations.

Presumably, tranilast binds to monomer conformations capable of docking onto growing fibrils, but not to actual fibril conformations, the two of which are thought to be different in the dock-and-lock scheme of $A\beta$ fibril growth.^{46–49} We propose the mechanisms depicted in Figure 6 for tranilast promotion of $A\beta$ fibril formation. $A\beta$ monomers exist in a dynamic equilibrium sampling multiple conformations (step 1). Tranilast binds to $A\beta$ monomers and stabilizes conformations compatible of binding to pre-existing fibrillar aggregates or creating new fibril seeds. These monomers then dock onto growing fibrils or to each other to

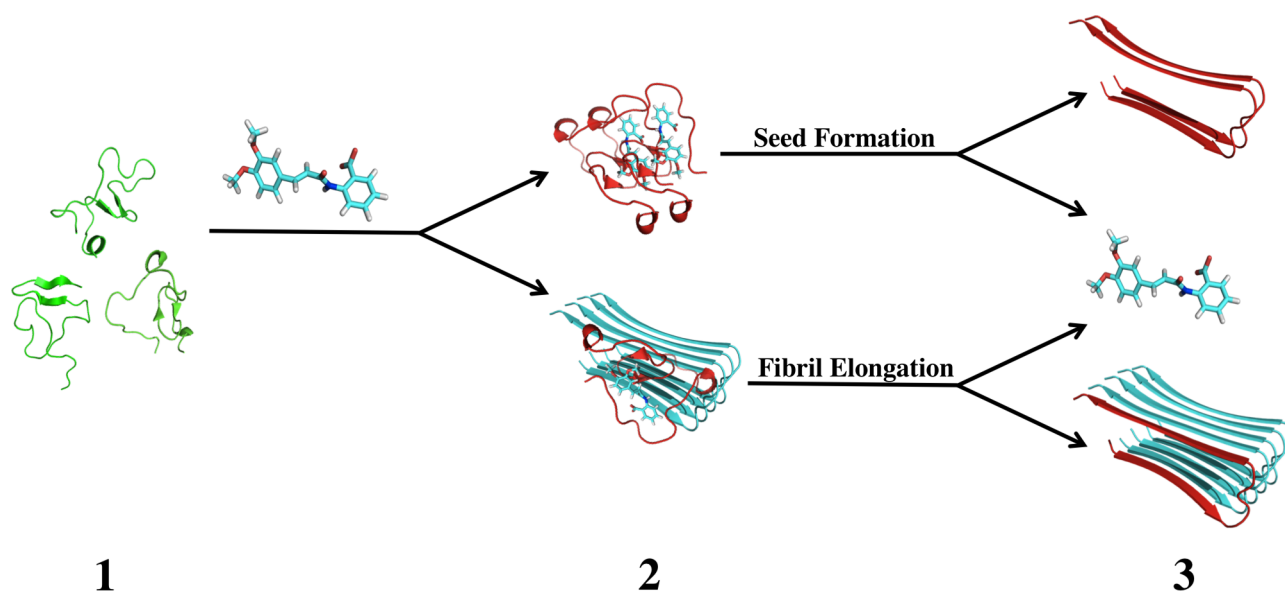


Figure 6. Proposed mechanism for tranilast binding to $A\beta$ monomers, explaining the increase in fibril formation. (1) $A\beta$ monomers (green) sample many different conformations in solution. (2) Tranilast binds to $A\beta$ monomers and stabilizes conformations (red) capable of docking onto fibrils (cyan) or creating fibril seeds, promoting fibril aggregation. (3) Upon locking onto the fibril or fibril seed, the $A\beta$ monomer adopts a new conformation, releasing tranilast and extending the aggregate.^{27,49}

create new fibril seeds (step 2). This docking leads to a conformational change that causes the monomer to lock onto the fibril or new seed, releasing tranilast for binding to another A β monomer (step 3). In this model, tranilast acts by promoting fibril elongation or seed formation with one tranilast molecule able to promote the incorporation of many A β monomers into the aggregates. This model can explain how despite having low binding affinity, tranilast has a large effect on A β fibril seeding and elongation.

■ ASSOCIATED CONTENT

● Supporting Information

The solubility of tranilast under the same buffer conditions used for the CSP titrations was confirmed by measuring a proportional increase in ¹H NMR to increasing tranilast concentration. Overlays of spectra from the CSP titrations are also presented, along with the fit curves for the 10 residues in each peptide that were used to determine K_d values. This material is available free of charge via the Internet at <http://pubs.acs.org>.

■ AUTHOR INFORMATION

Corresponding Author

*E-mail: wangc5@rpi.edu; phone: 518-276-3497.

Funding

This work was supported in part by University of California-Los Angeles Jim Easton Consortium for Alzheimer's Drug Discovery and Biomarker Development (G.B.); RJG Foundation Grant 2009S024 (G.B.); and a Cure Alzheimer's Fund Grant (G.B.).

Notes

The authors declare no competing financial interest.

■ REFERENCES

- (1) 2010 Alzheimer's Disease Facts and Figures, Executive Summary; Alzheimer's Association: Chicago, 2010.
- (2) Chong, Y. H., Shin, Y. J., Lee, E. O., Kaye, R., Glabe, C. G., and Tenner, A. J. (2006) ERK1/2 activation mediates Abeta oligomer-induced neurotoxicity via caspase-3 activation and tau cleavage in rat organotypic hippocampal slice cultures. *J. Biol. Chem.* 281, 20315–20325.
- (3) Masters, C. L., Cappai, R., Barnham, K. J., and Vilemagne, V. L. (2006) Molecular mechanisms for Alzheimer's disease: implications for neuroimaging and therapeutics. *J. Neurochem.* 97, 1700–1725.
- (4) Dahlgren, K. N., Manelli, A. M., Stine, W. B., Jr., Baker, L. K., Krafft, G. A., and LaDu, M. J. (2002) Oligomeric and fibrillar species of amyloid-beta peptides differentially affect neuronal viability. *J. Biol. Chem.* 277, 32046–32053.
- (5) Pike, C. J., Burdick, D., Walencewicz, A. J., Glabe, C. G., and Cotman, C. W. (1993) Neurodegeneration induced by beta-amyloid peptides in vitro: the role of peptide assembly state. *J. Neuroscience: Official J. Soc. Neurosci.* 13, 1676–1687.
- (6) Luhrs, T., Ritter, C., Adrian, M., Riek-Loher, D., Bohrmann, B., Döbeli, H., Schubert, D., and Riek, R. (2005) 3D structure of Alzheimer's amyloid-beta(1–42) fibrils. *Proc. Natl. Acad. Sci. U. S. A.* 102, 17342–17347.
- (7) Lorenzo, A., and Yankner, B. A. (1994) Beta-amyloid neurotoxicity requires fibril formation and is inhibited by congo red. *Proc. Natl. Acad. Sci. U. S. A.* 91, 12243–12247.
- (8) Harper, J. D., Wong, S. S., Lieber, C. M., and Lansbury, P. T. (1997) Observation of metastable Abeta amyloid protofibrils by atomic force microscopy. *Chem. Biol.* 4, 119–125.
- (9) Roher, A. E., Chaney, M. O., Kuo, Y. M., Webster, S. D., Stine, W. B., Haverkamp, L. J., Woods, A. S., Cotter, R. J., Tuohy, J. M., Krafft, G. A., Bonnell, B. S., and Emmerling, M. R. (1996) Morphology and toxicity of Abeta-(1–42) dimer derived from neuritic and vascular amyloid deposits of Alzheimer's disease. *J. Biol. Chem.* 271, 20631–20635.
- (10) Townsend, M., Shankar, G. M., Mehta, T., Walsh, D. M., and Selkoe, D. J. (2006) Effects of secreted oligomers of amyloid beta-protein on hippocampal synaptic plasticity: a potent role for trimers. *J. Physiol.* 572, 477–492.
- (11) Lesne, S., Koh, M. T., Kotilinek, L., Kaye, R., Glabe, C. G., Yang, A., Gallagher, M., and Ashe, K. H. (2006) A specific amyloid-beta protein assembly in the brain impairs memory. *Nature* 440, 352–357.
- (12) Barghorn, S., Biernat, J., and Mandelkow, E. (2005) Purification of recombinant tau protein and preparation of Alzheimer-paired helical filaments in vitro. *Methods Mol. Biol.* 299, 35–51.
- (13) Cummings, B. J., and Cotman, C. W. (1995) Image analysis of beta-amyloid load in Alzheimer's disease and relation to dementia severity. *Lancet* 346, 1524–1528.
- (14) Kuo, Y. M., Emmerling, M. R., Vigo-Pelfrey, C., Kasunic, T. C., Kirkpatrick, J. B., Murdoch, G. H., Ball, M. J., and Roher, A. E. (1996) Water-soluble Abeta (N-40, N-42) oligomers in normal and Alzheimer disease brains. *J. Biol. Chem.* 271, 4077–4081.
- (15) McLean, C. A., Cherny, R. A., Fraser, F. W., Fuller, S. J., Smith, M. J., Beyreuther, K., Bush, A. I., and Masters, C. L. (1999) Soluble pool of Abeta amyloid as a determinant of severity of neurodegeneration in Alzheimer's disease. *Ann. Neurol.* 46, 860–866.
- (16) Kato, T., and Tagami, H. (1986) Successful treatment of cheilitis granulomatosa with tranilast. *J. Dermatol.* 13, 402–403.
- (17) See, F., Watanabe, M., Kompa, A. R., Wang, B. H., Boyle, A. J., Kelly, D. J., Gilbert, R. E., and Krum, H. (2013) Early and Delayed Tranilast Treatment Reduces Pathological Fibrosis Following Myocardial Infarction. *Heart Lung Circ.* 22, 122–132.
- (18) Subramaniam, V., Ace, O., Prud'homme, G. J., and Jothy, S. (2011) Tranilast treatment decreases cell growth, migration and inhibits colony formation of human breast cancer cells. *Exp. Mol. Pathol.* 90, 116–122.
- (19) Rogosnitzky, M., Danks, R., and Kardash, E. (2012) Therapeutic potential of tranilast, an anti-allergy drug, in proliferative disorders. *Anticancer Res.* 32, 2471–2478.
- (20) Izumi, K., Mizokami, A., Li, Y. Q., Narimoto, K., Sugimoto, K., Kadono, Y., Kitagawa, Y., Konaka, H., Koh, E., Keller, E. T., and Namiki, M. (2009) Tranilast inhibits hormone refractory prostate cancer cell proliferation and suppresses transforming growth factor beta1-associated osteoblastic changes. *Prostate* 69, 1222–1234.
- (21) Chakrabarti, R., Subramaniam, V., Abdalla, S., Jothy, S., and Prud'homme, G. J. (2009) Tranilast inhibits the growth and metastasis of mammary carcinoma. *Anticancer Drugs* 20, 334–345.
- (22) Hiroi, M., Onda, M., Uchida, E., and Aimoto, T. (2002) Antitumor effect of N-[3,4-dimethoxycinnamoyl]-anthranilic acid (tranilast) on experimental pancreatic cancer. *J. Nippon Med. Sch.* 69, 224–234.
- (23) Schneider, A., Moraru, A., Krüger, C., Laage, R., Pitzer, C. (2011) Use Of Tranilast And Derivatives Thereof For The Therapy Of Neurological Conditions, United States Patent Application 20110112187, 2008.
- (24) Platten, M., Wild-Bode, C., Wick, W., Leitlein, J., Dichgans, J., and Weller, M. (2001) N-[3,4-Dimethoxycinnamoyl]-anthranilic acid (tranilast) inhibits transforming growth factor-beta release and reduces migration and invasiveness of human malignant glioma cells. *Int. J. Cancer* 93, 53–61.
- (25) Bitan, G., and Teplow, D. B. (2005) Preparation of aggregate-free, low molecular weight amyloid-beta for assembly and toxicity assays. *Methods Mol. Biol.* 299, 3–9.
- (26) Wang, C. (2011) Solution NMR studies of Abeta monomer dynamics. *Protein Peptide Lett.* 18, 354–361.
- (27) Sgourakis, N. G., Yan, Y., McCallum, S. A., Wang, C., and Garcia, A. E. (2007) The Alzheimer's peptides Abeta40 and 42 adopt distinct conformations in water: a combined MD/NMR study. *J. Mol. Biol.* 368, 1448–1457.

- (28) Wang, Y., Xiao, J., Suzek, T. O., Zhang, J., Wang, J., and Bryant, S. H. (2009) PubChem: a public information system for analyzing bioactivities of small molecules. *Nucleic Acids Res.* 37, W623–633.
- (29) *Molecular Operating Environment (MOE)*, 2012.10, Chemical Computing Group, I, Montreal, Quebec City, Canada.
- (30) Halgren, T. (1999) MMFF VI. MMFF94s option for energy minimization studies. *J. Comput. Chem.* 20, 720–729.
- (31) Sobolev, V., Sorokine, A., Prilusky, J., Abola, E. E., and Edelman, M. (1999) Automated analysis of interatomic contacts in proteins. *Bioinformatics* 15, 327–332.
- (32) Uno, K., Iijima, K., Koike, T., Abe, Y., Asano, N., Ara, N., and Shimosegawa, T. (2012) A pilot study of scheduled endoscopic balloon dilation with oral agent tranilast to improve the efficacy of stricture dilation after endoscopic submucosal dissection of the esophagus. *J. Clin. Gastroenterol.* 46, e76–82.
- (33) Prud'homme, G. J. (2012) Cancer stem cells and novel targets for antitumor strategies. *Curr. Pharm. Des.* 18, 2838–2849.
- (34) Kuba-Miyara, M., Agarie, K., Sakima, R., Imamura, S., Tsuchi, K., Yasumoto, T., Gima, S., Matsuzaki, G., and Ikehara, T. (2012) Inhibitory effects of an ellagic acid glucoside, okicamelliaside, on antigen-mediated degradation in rat basophilic leukemia RBL-2H3 cells and passive cutaneous anaphylaxis reaction in mice. *Int. Immunopharmacol.* 12, 675–681.
- (35) Jin, U. H., Lee, S. O., and Safe, S. (2012) Aryl hydrocarbon receptor (AHR)-active pharmaceuticals are selective AHR modulators in MDA-MB-468 and BT474 breast cancer cells. *J. Pharmacol. Exp. Ther.* 343, 333–341.
- (36) Glinka, Y., Mohammed, N., Subramaniam, V., Jothy, S., and Prud'homme, G. J. (2012) Neuropilin-1 is expressed by breast cancer stem-like cells and is linked to NF- κ B activation and tumor sphere formation. *Biochem. Biophys. Res. Commun.* 425, 775–780.
- (37) Subramaniam, V., Chakrabarti, R., Prud'homme, G. J., and Jothy, S. (2010) Tranilast inhibits cell proliferation and migration and promotes apoptosis in murine breast cancer. *Anticancer Drugs* 21, 351–361.
- (38) Sato, S., Takahashi, S., Asamoto, M., Naiki, T., Naiki-Ito, A., Asai, K., and Shirai, T. (2010) Tranilast suppresses prostate cancer growth and osteoclast differentiation in vivo and in vitro. *Prostate* 70, 229–238.
- (39) Prud'homme, G. J., Glinka, Y., Toulina, A., Ace, O., Subramaniam, V., and Jothy, S. (2010) Breast cancer stem-like cells are inhibited by a non-toxic aryl hydrocarbon receptor agonist. *PLoS One* 5, e13831.
- (40) Izumi, K., Mizokami, A., Shima, T., Narimoto, K., Sugimoto, K., Kobori, Y., Maeda, Y., Konaka, H., Koh, E., and Namiki, M. (2010) Preliminary results of tranilast treatment for patients with advanced castration-resistant prostate cancer. *Anticancer Res.* 30, 3077–3081.
- (41) Goto, T., Nemoto, T., Ogura, K., Hozumi, T., and Funata, N. (2010) Successful treatment of desmoid tumor of the chest wall with tranilast: a case report. *J. Med. Case Rep.* 4, 384.
- (42) Nakajima, K., Okita, Y., and Matsuda, S. (2004) Sensitivity of scirrhous gastric cancer to 5-fluorouracil and the role of cancer cell-stromal fibroblast interaction. *Oncol. Rep.* 12, 85–90.
- (43) Yashiro, M., Murahashi, K., Matsuoka, T., Nakazawa, K., Tanaka, H., Osaka, H., Koyama, T., Ohira, M., and Chung, K. H. (2003) Tranilast (N-3,4-dimethoxycyanomethyl anthranilic acid): a novel inhibitor of invasion-stimulating interaction between gastric cancer cells and orthotopic fibroblasts. *Anticancer Res.* 23, 3899–3904.
- (44) Noguchi, N., Kawashiri, S., Tanaka, A., Kato, K., and Nakaya, H. (2003) Effects of fibroblast growth inhibitor on proliferation and metastasis of oral squamous cell carcinoma. *Oral Oncol.* 39, 240–247.
- (45) Selkoe, D. J. (1994) Amyloid beta-protein precursor: new clues to the genesis of Alzheimer's disease. *Curr. Opin. Neurobiol.* 4, 708–716.
- (46) Krishnamoorthy, J., Brender, J. R., Vivekanandan, S., Jahr, N., and Ramamoorthy, A. (2012) Side-chain dynamics reveals transient association of A β (1–40) monomers with amyloid fibers. *J. Phys. Chem. B* 116, 13618–13623.
- (47) Straub, J. E., and Thirumalai, D. (2010) Principles governing oligomer formation in amyloidogenic peptides. *Curr. Opin. Struct. Biol.* 20, 187–195.
- (48) Massi, F., and Straub, J. E. (2001) Energy landscape theory for Alzheimer's amyloid beta-peptide fibril elongation. *Proteins* 42, 217–229.
- (49) Esler, W. P., Stimson, E. R., Jennings, J. M., Vinters, H. V., Ghilardi, J. R., Lee, J. P., Mantyh, P. W., and Maggio, J. E. (2000) Alzheimer's disease amyloid propagation by a template-dependent dock-lock mechanism. *Biochemistry* 39, 6288–6295.
- (50) Tolcher, A. W., Messersmith, W. A., Mikulski, S. M., Papadopoulos, K. P., Kwak, E. L., Gibbon, D. G., Patnaik, A., Falchook, G. S., Dasari, A., Shapiro, G. I., Boylan, J. F., Xu, Z. X., Wang, K., Koehler, A., Song, J., Middleton, S. A., Deutsch, J., Demario, M., Kurzrock, R., and Wheler, J. J. (2012) Phase I study of RO4929097, a gamma secretase inhibitor of Notch signaling, in patients with refractory metastatic or locally advanced solid tumors. *J. Clin. Oncol.* 30, 2348–2353.
- (51) Tong, G., Wang, J. S., Sverdlov, O., Huang, S. P., Slemmon, R., Croop, R., Castaneda, L., Gu, H., Wong, O., Li, H., Berman, R. M., Smith, C., Albright, C. F., and Dockens, R. (2013) A contrast in safety, pharmacokinetics and pharmacodynamics across age groups after a single 50 mg oral dose of the gamma-secretase inhibitor avagacestat. *Br. J. Clin. Pharmacol.* 75, 136–145.
- (52) Xia, W., Wong, S. T., Hanlon, E., and Morin, P. (2012) gamma-secretase modulator in Alzheimer's disease: shifting the end. *J. Alzheimer's Dis.: JAD* 31, 685–696.
- (53) Chang, L., Bakhos, L., Wang, Z., Venton, D. L., and Klein, W. L. (2003) Femtomole immunodetection of synthetic and endogenous amyloid-beta oligomers and its application to Alzheimer's disease drug candidate screening. *J. Mol. Neurosci.* 20, 305–313.
- (54) Dovey, H. F., John, V., Anderson, J. P., Chen, L. Z., de Saint Andrieu, P., Fang, L. Y., Freedman, S. B., Folmer, B., Goldbach, E., Holsztyńska, E. J., Hu, K. L., Johnson-Wood, K. L., Kennedy, S. L., Kholodenko, D., Knops, J. E., Latimer, L. H., Lee, M., Liao, Z., Lieberburg, I. M., Motter, R. N., Mutter, L. C., Nietz, J., Quinn, K. P., Sacchi, K. L., Seubert, P. A., Shopp, G. M., Thorsett, E. D., Tung, J. S., Wu, J., Yang, S., Yin, C. T., Schenk, D. B., May, P. C., Altstiel, L. D., Bender, M. H., Boggs, L. N., Britton, T. C., Clemens, J. C., Czilli, D. L., Dieckman-McGinty, D. K., Droste, J. J., Fuson, K. S., Gitter, B. D., Hyslop, P. A., Johnstone, E. M., Li, W. Y., Little, S. P., Mabry, T. E., Miller, F. D., and Audia, J. E. (2001) Functional gamma-secretase inhibitors reduce beta-amyloid peptide levels in brain. *J. Neurochem.* 76, 173–181.
- (55) Baures, P. W., Peterson, S. A., and Kelly, J. W. (1998) Discovering transthyretin amyloid fibril inhibitors by limited screening. *Bioorg. Med. Chem.* 6, 1389–1401.
- (56) Isvoran, A., Badel, A., Craescu, C. T., Miron, S., and Miteva, M. A. (2011) Exploring NMR ensembles of calcium binding proteins: perspectives to design inhibitors of protein-protein interactions. *BMC Struct. Biol.* 11, 24.
- (57) Kawatkar, S., Moustakas, D., Miller, M., and Joseph-McCarthy, D. (2012) Virtual fragment screening: exploration of MM-PBSA re-scoring. *J. Comput.-Aided Mol. Des.* 26, 921–934.
- (58) Stark, J. L., and Powers, R. (2012) Application of NMR and molecular docking in structure-based drug discovery. *Top. Curr. Chem.* 326, 1–34.
- (59) Ai, R., and Chang, C. E. (2012) Ligand-specific homology modeling of human cannabinoid (CB1) receptor. *J. Mol. Graphics Modell.* 38, 155–164.
- (60) Rungsardthong, K., Mares-Samano, S., and Penny, J. (2012) Virtual screening of ABCC1 transporter nucleotidebinding domains as a therapeutic target in multidrug resistant cancer. *Bioinformation* 8, 907–911.
- (61) Skariyachan, S., Mahajanakatti, A. B., Sharma, N., Karanth, S., Rao, S., and Rajeswari, N. (2012) Structure based virtual screening of novel inhibitors against multidrug resistant superbugs. *Bioinformation* 8, 420–425.

(62) Strambi, A., Mori, M., Rossi, M., Colecchia, D., Manetti, F., Carlomagno, F., Botta, M., and Chiariello, M. (2013) Structure Prediction and Validation of the ERK8 Kinase Domain. *PloS One* 8, e52011.

(63) Wadood, A., and Ulhaq, Z. (2013) In silico identification of novel inhibitors against *Plasmodium falciparum* dihydroorate dehydrogenase. *J. Mol. Graphics Modell.* 40, 40–47.

(64) Park, I. H., and Li, C. (2010) Dynamic ligand-induced-fit simulation via enhanced conformational samplings and ensemble dockings: a survivin example. *J. Phys. Chem. B* 114, 5144–5153.